

Robotic sanding system for new designed furniture with free-formed surface

Fusaomi Nagata^{a,*}, Yukihiro Kusumoto^b, Yoshihiro Fujimoto^b, Keigo Watanabe^c

^aDepartment of Electronics and Computer Science, Tokyo University of Science, Yamaguchi, Daigaku-Dori 1-1-1, Sanyo-Onoda 756-0884, Japan

^bInterior & Design Research Institute, Fukuoka Industrial Technology Center, Agemaki 405-3, Ohkawa, Fukuoka 831-0031, Japan

^cDepartment of Advanced Systems Control Engineering, Graduate School of Science and Engineering, Saga University, Honjomachi 1, Saga 840-8502, Japan

Received 10 December 2005; received in revised form 10 March 2006; accepted 7 April 2006

Abstract

In this paper, a sanding system based on an industrial robot with a surface following controller is proposed for the sanding process of wooden materials constructing furniture. Handy air-driven tools can be easily attached to the tip of the robot arm via a compact force sensor. The robotic sanding system is called the 3D robot sander. The robot sander has two novel features. One is that the polishing force acting between the tool and wooden workpiece is delicately controlled to track a desired value, e.g., 2 kgf. The polishing force is defined as the resultant force of the contact force and kinetic friction force. The other is that no complicated teaching operation is required to obtain a desired trajectory of the tool. Cutter location (CL) data, which are tool paths generated by a CAD/CAM system, are directly used for the basic trajectory of the handy tool attached to the robot arm. The robot sander can be applied to the sanding task of free-formed curved surface with which conventional sanding machines have not been able to cope. The effectiveness and promise are shown and discussed through a few experiments.

© 2006 Elsevier Ltd. All rights reserved.

Keywords: Robotic sanding; CAD/CAM; Cutter location data; Non-taught operation; Surface following control; Polishing force

1. Introduction

In manufacturing industry of wooden furniture, CAD/CAM systems and NC machine tools have been introduced widely and generally, so that the design and machining processes are rationalized drastically. However, the sanding process after machining is hardly automated yet, because it requires delicate and dexterous skills so as not to spoil the beauty and quality of the surface. Up to now, several sanding machines have been developed for wooden materials. For example, the wide belt sander as shown in Fig. 1 is used for flat workpieces constructing furniture. The profile sander as shown in Fig. 2 is suitable for the sanding around the edge. However, these conventional machines cannot be applied to the sanding task of the workpiece with free-formed surface. Accordingly, we must depend on skilled workers who can not only perform

appropriate force control of sanding tools but also deal with complex curved surface as shown in Fig. 3. Skilled workers usually use handy air-driven tools such as a double action sanding tool and an orbital sanding tool as shown in Fig. 4. In order to produce a better surface quality, the double action sander simultaneously performs rotational and eccentric motions. As can be guessed, such tools spread out unhealthy noise, vibration and dust. The most serious problem in the sanding process is that the sanding task in such a bad working environment is extremely hard for skilled workers. From this reason, an advanced sanding machine which can even partially replace the skilled workers is being required in the furniture manufacturing industry.

Industrial robots have been progressed remarkably and applied to several tasks such as painting, welding, handling and so on. In these cases, it is important to precisely control the position of the end-effector attached to the tip of the robot arm. On the contrary, when the robots are applied to polishing, deburring or grinding task, it is

*Corresponding author. Tel.: +81 836 88 4547; fax: +81 836 88 3400.
E-mail address: nagata@ed.yama.tus.ac.jp (F. Nagata).

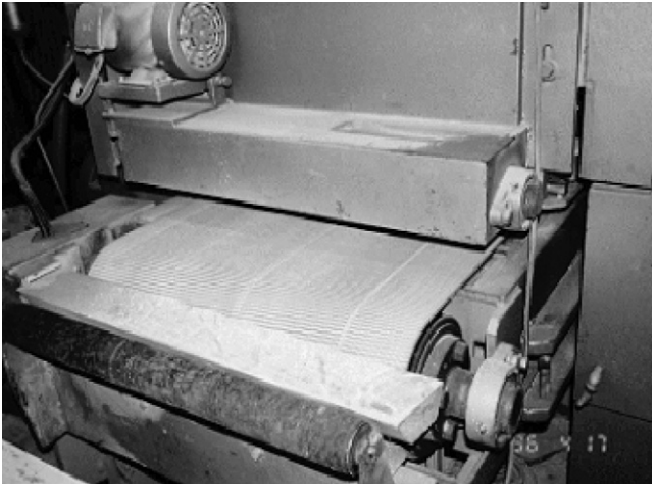


Fig. 1. Conventional wide belt sander.

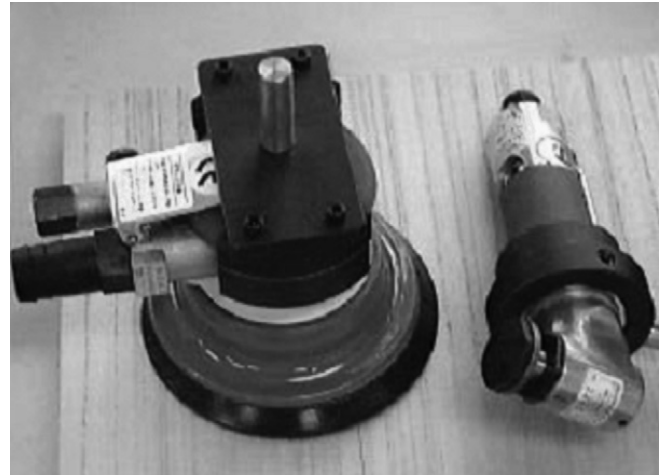


Fig. 4. Handy air-driven sanding tools usually used by skilled workers.



Fig. 2. Conventional profile sander.



Fig. 3. Sanding scene by a skilled worker.

indispensable to use some force control strategy without damaging the object. For example, polishing robots and finishing robots were presented in [1–5]. Automated robotic deburring and grinding were also introduced in [6–10].

Two representative force control methods have been ever proposed. They are impedance control [11] and hybrid position/force control [12]. The impedance control is one of the most effective strategies for a manipulator to desirably reduce or absorb the impact force with an object. It is characterized by an ability that controls the mechanical impedance such as inertia, damping and stiffness acting between the end-effector and its environment. The impedance control does not have a force control mode or a position control mode but it is a combination of the force and velocity of the end-effector. On the other hand, the hybrid position/force control method simultaneously controls the position and force of a robot manipulator. However, the six constraints which consist of 3-DOF positions and 3-DOF forces in a constrained frame cannot be simultaneously satisfied. In order to avoid the interference between the force control system and position control system, either force control mode or position control mode is selected in each direction.

Surface following control is a basic sanding strategy for industrial robots. It is known that two control schemes are needed to realize the surface following control system. One is the position/orientation control of the sanding tool attached to the tip of the robot arm. The other is the force control to stably keep in contact along the curved surface of the workpiece. It should be noted that if the geometric information on the workpiece is unknown, then it is so difficult to satisfactorily control the contact force moving with a higher speed [13]. To suppress overshoots and oscillations, for example, the feed rate must be given a small value. Furthermore, it is also difficult to control the orientation of the sanding tool, keeping in contact with the workpiece from normal direction.

The authors have conducted relevant fundamental studies. As for force control, impedance model following force control method was proposed for an industrial robot with open architecture concept [14]. The force controller adjusts the contact force acting between a sanding tool and workpiece through a desired impedance model. In [15], fuzzy environment model was presented for environments with unknown physical property. The fuzzy environment model is learned with genetic algorithm and can estimate the stiffness of unknown environment. The effectiveness was evaluated through simulations using a dynamic model of PUMA560 manipulator. In [16], a gravity compensator was considered to remove the influence of tool weight from measured force. In [17], concerning tool position and orientation control, it was further considered how to realize non-taught operation for industrial robots. Furthermore, hyper CL data were also presented to deal with new statements about the regulation of sanding parameters in [18].

In this paper, a robotic sanding system is integrated for new designed furniture with free-formed curved surface. The robotic sanding system provides a practical surface following control that allows industrial robots not only to adjust the polishing force through a desired impedance model in Cartesian space but also to follow a curved surface keeping contact with from normal direction. The polishing force is assumed to be the resultant force of contact force and kinetic friction force. We also describe how to apply the sanding system to a sanding task of wooden workpiece without complicated teaching process. A few sanding experiments are shown to demonstrate the effectiveness and promise of the proposed robotic sanding system using the surface following controller.

2. Robotic sanding system

Recently, open architectural industrial robots have been proposed to comply with user's various requests with regard to application developments. The industrial robot has an open programming interface for Windows or Linux,

so that we can try to program new functions such as force control, compliance control and so on. The 6-DOF industrial robot shown in Fig. 5 is a FS20N with a PC-based controller provided by Kawasaki Heavy Industries. The proposed robotic sanding system is developed based on the industrial robot whose tip has a compact force sensor. A handy sanding tool can be easily attached to the tip of the robot arm via the force sensor. A PC is connected to the PC-based controller via an optical fiber cable. The PC-based controller provides several Windows API (application programming interface) functions, such as servo control with joint angles, forward/inverse kinematics and so on. By using such API functions, for instance, the position and orientation at the tip of the robot arm can be controlled easily and safely. In the following section, the surface following controller is implemented for robotic sanding by using the Windows API functions.

3. Surface following control for robotic sanding system

The robotic sanding system has two main features: one is that neither conventional complicated teaching tasks nor post-processor (CL data → NC data) is required; the other is that the polishing force acting on the sanding tool and tool position/orientation are simultaneously controlled along free-formed curved surface. In this section, a surface following control method indispensable for realizing the features are described in detail.

3.1. Desired trajectory

Robotic sanding task needs a desired trajectory so that the sanding tool attached to the tip of the robot arm can follow the object's surface, keeping contact with the surface from the normal direction. In executing a motion using an industrial robot, the trajectory is generally obtained in advance, e.g., through conventional robot teaching process. When the conventional teaching for an object with complex curved surface is conducted, the operator has to input a large number of teaching points along the surface.

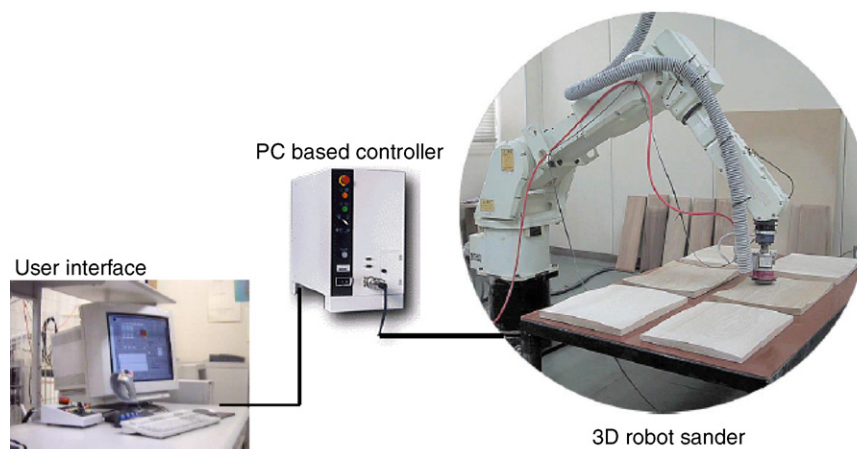


Fig. 5. Robotic sanding system developed based on an open architectural industrial robot FS20N.

Such a teaching task is complicated and time-consuming. However, if the object is fortunately designed and manufactured by a CAD/CAM system and an NC machine tool, then the CL data can be referred as the desired trajectory. In order to realize non-taught operation, we have already proposed a generalized trajectory generator [19,20] using the CL data, which yields the desired trajectory $\mathbf{r}(k)$ at the discrete time k given by

$$\mathbf{r}(k) = [\mathbf{x}_d^T(k) \ \mathbf{o}_d^T(k)]^T, \quad (1)$$

where $\mathbf{x}_d(k) = [x_{dx}(k) \ x_{dy}(k) \ x_{dz}(k)]^T$ and $\mathbf{o}_d(k) = [o_{d\alpha}(k) \ o_{d\beta}(k) \ o_{d\gamma}(k)]^T$ are the position and orientation components, respectively. $\mathbf{o}_d(k)$ is the normal vector at the position $\mathbf{x}_d(k)$. In the following, we detail how to make $\mathbf{r}(k)$ using the CL data.

A target workpiece with curved surface is generally designed by a 3D CAD/CAM, so that the CL data can be calculated by the main-processor of the CAM. The CL data are sequential points along the model surface given by a zigzag path or a whirl path. In this approach, the desired trajectory $\mathbf{r}(k)$ is generated along the CL data. The CL data are usually calculated with a linear approximation along the model surface. The i th step is written by

$$\mathbf{CL}(i) = [p_x(i) \ p_y(i) \ p_z(i) \ n_x(i) \ n_y(i) \ n_z(i)]^T, \quad (2)$$

$$\{n_x(i)\}^2 + \{n_y(i)\}^2 + \{n_z(i)\}^2 = 1, \quad (3)$$

where $\mathbf{p}(i) = [p_x(i) \ p_y(i) \ p_z(i)]^T$ and $\mathbf{n}(i) = [n_x(i) \ n_y(i) \ n_z(i)]^T$ are position and orientation vectors, respectively. $\mathbf{r}(k)$ is obtained by using linear equations and a tangential velocity $\mathbf{v}_t(k)$ represented by

$$\mathbf{v}_t(k) = [v_{tx}(k) \ v_{ty}(k) \ v_{tz}(k)]^T. \quad (4)$$

A relation between $\mathbf{CL}(i)$ and $\mathbf{r}(k)$ is shown in Fig. 6. In this case, assuming $\mathbf{r}(k) \in [\mathbf{CL}(i), \mathbf{CL}(i+1)]$ we obtain $\mathbf{r}(k)$ through the following procedure. First, a direction vector $\mathbf{t}(i)$ is given by

$$\mathbf{t}(i) = \mathbf{p}(i+1) - \mathbf{p}(i) \quad (5)$$

so that each component of $\mathbf{v}_t(k)$ is obtained by

$$v_{tj}(k) = \|\mathbf{v}_t(k)\| \frac{t_j(i)}{\|\mathbf{t}(i)\|} \quad (j = x, y, z). \quad (6)$$

Using a sampling width Δt , each component of the desired position $\mathbf{x}_d(k)$ is given by

$$x_{dj}(k) = x_{dj}(k-1) + v_{tj}(k)\Delta t \quad (j = x, y, z). \quad (7)$$

Next, the desired orientation $\mathbf{o}_d(k)$ is considered. We define two angles $\theta_1(i), \theta_2(i)$ as shown in Fig. 7. $\theta_1(i)$ and $\theta_2(i)$ are the tool angles of inclination and rotation, respectively. Using $\theta_1(i)$ and $\theta_2(i)$, each component of $\mathbf{n}(i)$ is represented by

$$\alpha(i) = \sin \theta_1(i) \cos \theta_2(i), \quad (8)$$

$$\beta(i) = \sin \theta_1(i) \sin \theta_2(i), \quad (9)$$

$$\gamma(i) = \cos \theta_1(i). \quad (10)$$

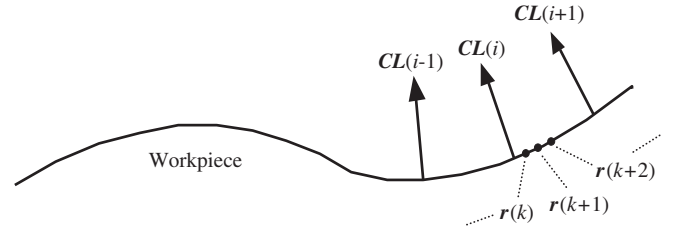


Fig. 6. Relation between CL data $\mathbf{CL}(i)$ and desired trajectory $\mathbf{r}(k)$.

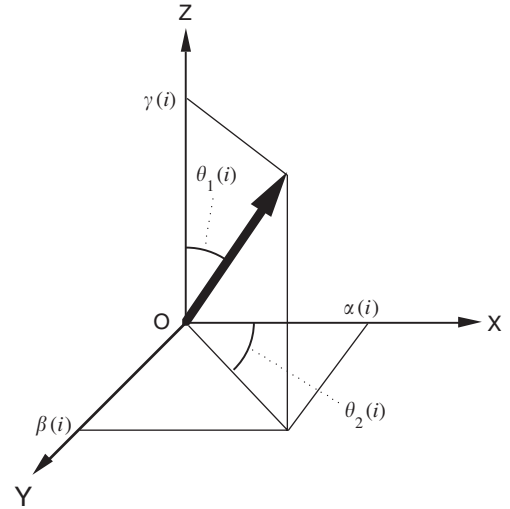


Fig. 7. Normalized tool vector $\mathbf{n}(i)$ represented by $\theta_1(i)$ and $\theta_2(i)$ in robot base coordinate system.

The desired tool angles $\theta_{r1}(k), \theta_{r2}(k)$ of inclination and rotation at the discrete time k can be calculated as

$$\theta_{rj}(k) = \theta_j(i) + \{\theta_j(i+1) - \theta_j(i)\} \frac{\|\mathbf{x}_d(k) - \mathbf{p}(i)\|}{\|\mathbf{t}(i)\|}, \quad (11)$$

where $j = 1, 2$. If (11) is substituted into (8), (9), (10), we finally obtain

$$o_{d\alpha}(k) = \sin \theta_{r1}(k) \cos \theta_{r2}(k), \quad (12)$$

$$o_{d\beta}(k) = \sin \theta_{r1}(k) \sin \theta_{r2}(k), \quad (13)$$

$$o_{d\gamma}(k) = \cos \theta_{r1}(k). \quad (14)$$

$\mathbf{x}_d(k)$ and $\mathbf{o}_d(k)$ mentioned above are directly obtained from the CL data without any conventional complicated teaching, and used for the desired position and orientation of a sanding tool attached to a robot arm.

3.2. Polishing force

In this section, a sanding strategy dealing with polishing force is described in detail. The polishing force vector $\mathbf{F}(k) = [F_x(k) \ F_y(k) \ F_z(k)]^T$ is assumed to be the resultant force of contact force vector $\mathbf{f}(k) = [f_x(k) \ f_y(k) \ f_z(k)]^T$ and kinetic friction force vector $\mathbf{F}_r(k) = [F_{rx}(k) \ F_{ry}(k) \ F_{rz}(k)]^T$ that are given to the workpiece as shown

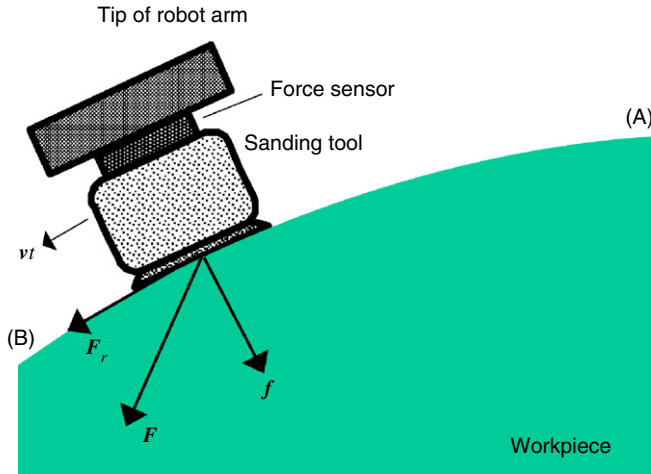


Fig. 8. Polishing force $F(k)$ composed of contact force $f(k)$ and kinetic friction force $F_r(k)$.

in Fig 8, where the sanding tool is moving along on the surface from (A) to (B). $F_r(k)$ is written by

$$F_r(k) = \text{diag}(\mu_x, \mu_y, \mu_z) \|f(k)\| \frac{v_t(k)}{\|v_t(k)\|} + \text{diag}(\eta_x, \eta_y, \eta_z) v_t(k), \quad (15)$$

where $\text{diag}(\mu_x, \mu_y, \mu_z) \|f(k)\| (v_t(k) / \|v_t(k)\|)$ is the Coulomb friction, and $\text{diag}(\eta_x, \eta_y, \eta_z) v_t(k)$ is the viscous friction. μ_i and η_i ($i = x, y, z$) are the i -directional coefficients of Coulomb friction per unit contact force and of viscous friction, respectively. Each friction force is generated by $f(k)$ and $v_t(k)$, respectively. $F(k)$ is represented by

$$F(k) = f(k) + F_r(k). \quad (16)$$

The polishing force magnitude can be easily measured by using a 3-DOF force sensor attached between the tip of the arm and the sanding tool, which is given by

$$\|F(k)\| = \sqrt{\{^S F_x(k)\}^2 + \{^S F_y(k)\}^2 + \{^S F_z(k)\}^2}, \quad (17)$$

where $^S F_x(k)$, $^S F_y(k)$ and $^S F_z(k)$ are the each directional component of force sensor measurements in sensor coordinate system. In the following section, the error $E_f(k)$ of polishing force magnitude is calculated by

$$E_f(k) = F_d - \|F(k)\|, \quad (18)$$

where F_d is a desired polishing force.

3.3. Feedback control of polishing force

In the manufacturing industry of wooden furniture, skilled workers usually use handy air-driven tools to finish the surface after machining or painting. These types of tools cause high frequency and large magnitude vibrations, so that it is so difficult for the skilled workers to sand the workpiece keeping the polishing force a desired value. Consequently, undesirable unevenness tends to appear on the sanded surface. In order to achieve a good surface

finishing, it is fundamental and effective to stably control the polishing force. When the robotic sanding system runs, the polishing force is controlled by the impedance model following force control with integral action given by

$$v_{\text{normal}}(k) = v_{\text{normal}}(k-1)e^{-(B_d/M_d)\Delta t} + (e^{-(B_d/M_d)\Delta t} - 1) \frac{K_f}{B_d} E_f(k) + K_{fi} \sum_{n=1}^k E_f(n), \quad (19)$$

where $v_{\text{normal}}(k)$ is the velocity scalar; K_f is the force feedback gain; K_{fi} is the integral control gain; M_d and B_d are the desired mass and desired damping coefficients, respectively. Δt is the sampling width. Using $v_{\text{normal}}(k)$, the normal velocity vector $v_n(k) = [v_{nx}(k) \ v_{ny}(k) \ v_{nz}(k)]$ at the center of the contact point is represented by

$$v_n(k) = v_{\text{normal}}(k) \frac{o_d(k)}{\|o_d(k)\|}. \quad (20)$$

3.4. Feedforward and feedback control of position

Currently, wooden furniture are designed and machined with 3D CAD/CAM systems and NC machine tools, respectively. Accordingly the CL data generated from the main-processor of the CAM can be used for the desired trajectory of the sanding tool. The tool path (CL data) as shown in Fig. 9, which are calculated in advance based on a zigzag path, is considered to be a desired trajectory of the sanding tool. Fig. 10 shows the block diagram of the surface following controller implemented in the robot sander. The position and orientation of the tool attached to the tip of the robot arm are feedforwardly controlled by the tangential velocity $v_t(k)$ and rotational velocity $v_r(k)$, respectively, referring $x_d(k)$ and $o_d(k)$. $v_t(k)$ is given through an open-loop action so as not to interfere with the force feedback loop. The polishing force is regulated by $v_n(k)$ which is perpendicular to $v_t(k)$. $v_n(k)$ is given to the normal direction referring the orientation vector $o_d(k)$.

It should be noted, however, that using only $v_t(k)$ is not enough to precisely carry out desired trajectory control along the CL data: actual trajectory tends to deviate from

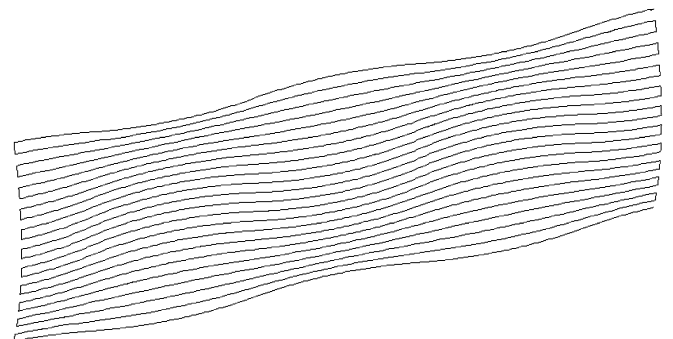


Fig. 9. Zigzag path generated from main-processor of CAM.

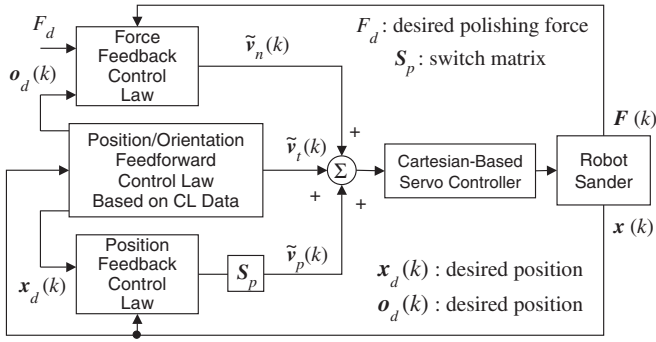


Fig. 10. Block diagram of the surface following controller implemented in the robot sander.

the desired one, so that the constant pick feed (e.g., 20 mm) cannot be performed. This undesirable phenomenon leads to the lack of uniformity on the surface. To overcome this problem, a simple position feedback loop with small gains is added as shown in Fig. 10 so that the tool does not deviate from the desired pick feed. The position feedback control law generates another velocity $v_p(k)$ given by

$$v_p(k) = S_p \left\{ K_p E_p(k) + K_i \sum_{n=1}^k E_p(n) \right\}, \quad (21)$$

where $S_p = \text{diag}(S_x, S_y, S_z)$ is a switch matrix to realize a weak coupling control in each direction. If $S_p = \text{diag}(1, 1, 1)$, then the coupling control is active in all directions; whereas if $S_p = \text{diag}(0, 0, 0)$, then the position feedback loop does not contribute to the force feedback loop in all directions. $E_p(k) = x_d(k) - x(k)$ is the position error vector. $x(k)$ is the current position of the sanding tool attached to the tip of the arm and is obtained from the forward kinematics of the robot. $K_p = \text{diag}(K_{px}, K_{py}, K_{pz})$ and $K_i = \text{diag}(K_{ix}, K_{iy}, K_{iz})$ are the position feedback gain and its integral gain matrices, respectively. Each component of K_p and K_i must be set to small values so as not to obviously disturb the force control loop. Finally, recomposed velocities $\tilde{v}_n(k) = [v_n^T(k) \ 0 \ 0 \ 0]^T$, $\tilde{v}_t(k) = [v_t^T(k) \ v_r^T(k)]^T$ and $\tilde{v}_p(k) = [v_p^T(k) \ 0 \ 0 \ 0]^T$ are summed up, and those of which are given to the reference of the Cartesian-based servo controller of the industrial robot.

It is known that the six constraints, which consist of 3-DOF positions and 3-DOF forces in a constraint frame, cannot be simultaneously satisfied [21]. However, the delicate cooperation between the position feedback loop and force feedback loop is an important key point to successfully achieve a robotic sanding with curved surface.

3.5. Hyper CL data

One of the features of the robot sander is that the CL data are referred as the desired trajectory of the sanding tool attached to the tip of the arm. Therefore, the complicated teaching process can be completely omitted. It is also useful that no post-processor included in CAM is

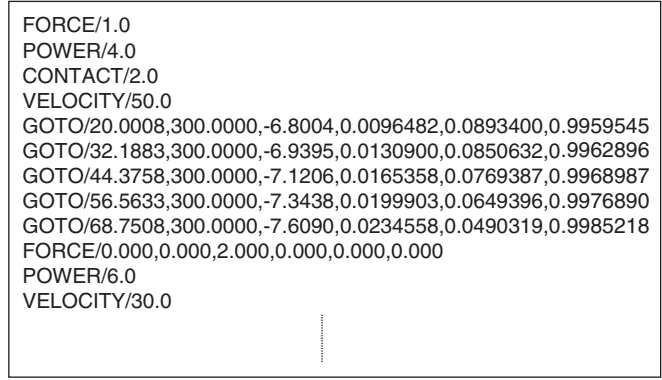


Fig. 11. Example of proposed hyper CL data.

required to transform the CL data into the NC data, i.e., the robot sander does not run based on the NC data but the CL data. The conventional CL data mainly deal with static positions and orientations along the curved surface of a model. In order to realize such a skillful sanding as skilled workers perform, we propose hyper CL data that can describe serviceable items as shown in Fig. 11. For example, following conditions can be specified:

- (1) Desired polishing force acting between a sanding tool and a workpiece;
- (2) Sanding power such as motor torque or air pressure;
- (3) Feed rate (velocity tangential to curved surface);
- (4) Task mode change (contact mode \leftrightarrow non-contact mode), etc.

The desired polishing force F_d kgf is recognized by

$$\text{FORCE}/F_d. \quad (22)$$

The air pressure P kgf/cm² of an air-driven sanding tool is regulated by

$$\text{POWER}/P. \quad (23)$$

The feed rate norm $\|v_t\|$ mm/s in contact state is set by

$$\text{VELOCITY}/\|v_t\|. \quad (24)$$

The task mode change from contact mode to non-contact mode is switched by

$$\text{NON-CONTACT}/v_m, d, \quad (25)$$

where the sanding tool takes off from the workpiece with v_m mm/s to the normal direction; d mm is the distance to be moved. On the other hand, the task mode change from non-contact mode to contact mode is switched by

$$\text{CONTACT}/v, \quad (26)$$

where v mm/s is the approaching velocity from the normal direction. Due to the hyper CL data, it has been possible to detailedly record sanding skills.



Fig. 12. An example of curved workpiece that conventional sanding machines cannot deal with.

4. Experimental results

In this section, experimental results of surface sanding experiment are given by using the proposed robot sander. The orbital sanding tool is widely used by skilled workers to sand or finish a workpiece with curved surface. The base of the orbital sanding tool can perform eccentric motion. That is the reason that the orbital sander is not only a powerful sanding tool but also gives good surface finishing with less scratches. In this experiment, an orbital sanding tool is selected and attached to the tip of the robot arm via a force sensor. The size of the base and the eccentricity are 75 × 110 mm and 4 mm, respectively. The weight of the sanding tool is 800 g. When a sanding task is conducted, a circular pad with a sanding paper is attached to the base.

Fig. 12 shows an example of the target workpieces after NC machining, which is a representative shape that the conventional sanding machines cannot sand sufficiently. The pick feed in the NC machining is set to 3 mm. The workpiece before sanding shown in Fig. 12 has undesirable cusp marks higher than 1 mm every pick feed. The robot sander first removed the cusp marks using a rough sanding paper #80, then sanded the surface using a sanding paper with a middle roughness #220 and finally a smooth paper #400. The diameters of the pad and paper were cut to 65 mm, which were so larger than that of the ball-end mill (17 mm) used in the NC machining process. Therefore, we regenerated the CL data with a pick feed 15 mm for the robotic sanding as shown in Fig. 9 and substituted the CL data for the controller shown in Fig. 10. The contour was made so as to be a small size with an offset 15 mm to prevent the edge of the workpiece from over sanding. Table 1 shows the other sanding conditions and the parameters of the surface following controller shown in Fig. 10. These semi-optimum values were found through trial and error.

Fig. 13 shows the sanding scene using the robot sander. In this case, the polishing force was controlled as shown in Fig. 14. Handy air-driven tools are usually used by skilled

Table 1
Sanding conditions and control parameters

Conditions or parameters	Values
Workpiece	Japanese oak
Size (mm)	1200 × 425 × 85
Diameter of sand paper (mm)	65
Grain size of sandpaper	80 → 220 → 400
Desired polishing force F_d (kgf)	1.0
Feed rate $\ v_t\ $ (mm/s)	30
Pick feed of CL data (mm)	15
Air pressure of orbital sanding tool (kgf/cm ²)	4.0
Desired mass coefficient M_d (kgf s ² /mm)	0.01
Desired damping coefficient B_d (kgf s/mm)	20
Force feedback gain K_f	1
Integral control gain for polishing force K_{fi}	0.001
Switch matrix for weak coupling control S_p	diag(0, 1, 0)
Position feedback gain matrix K_p	diag(0, 0.01, 0)
Integral control gain matrix K_i for position	diag(0, 0.0001, 0)
Sampling width Δt (ms)	0.01

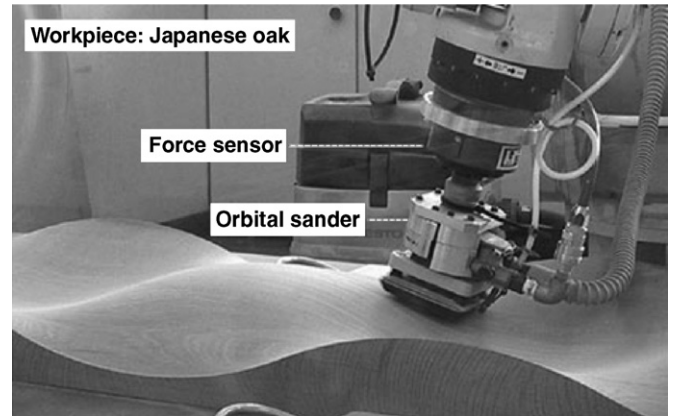


Fig. 13. Sanding scene using an orbital sanding tool.

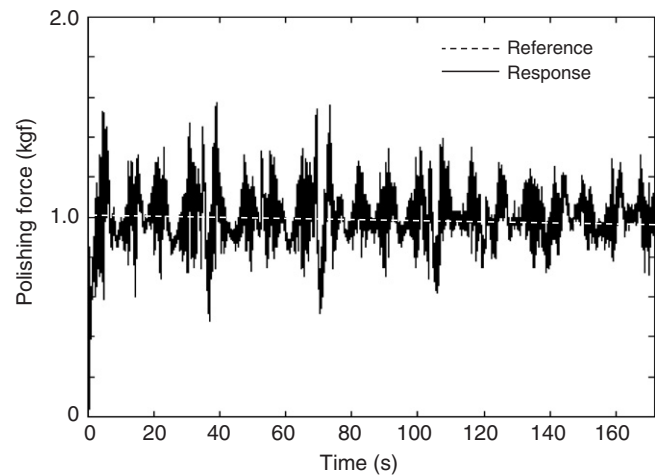


Fig. 14. An example of time history of polishing force.

workers to sand wooden material constructing furniture. These types of tools cause large noise and vibration. Further, the system of force control consists of an



Fig. 15. Sanding scene of wooden table with curved surface.



Fig. 16. Bench with curved surface.

industrial robot, force sensor, attachment, handy air-driven tool, zig and wooden material. Because each of them has stiff property, it is not easy to strictly keep the polishing force a constant value without overshoot and oscillation. That is the reason why measured value of the polishing force tends to have spikes and noise as shown in Fig. 14. However, the result would be much better than the one by skilled workers. Although it is so difficult and hard for skilled workers to simultaneously keep the polishing force, tool position and orientation to be desired situation even for a few minutes, the robot sander can perform the task more uniformly and perseveringly.

Another sanding scene of the wooden table with curved surface is also shown in Fig. 15. The touch feelings with both the fingers and the palm were very satisfactory. Undesirable cusp marks were not observed at all. And also, there was no over sanding around the edge of the workpiece and no swell on the surface. Furthermore, we conducted a quantitative evaluation by using a stylus instrument, so that the measurements obtained by the arithmetical mean roughness (Ra) and max height (Ry) were around 1 and 3 μm , respectively.

Figs. 16 and 17 show new designed furniture using the workpiece sanded by the robot sander. It was confirmed from the experimental results that the proposed robotic sanding system could successfully sand the woody workpieces with curved surface.

5. Conclusions and future work

This paper has dealt with a robotic sanding system for attractively designed furniture with free-formed surface. The system has been developed using an industrial robot with an open architectural controller. The system has two novel features. One is that the surface following controller developed for robotic sanding allows the robot to simultaneously realize a delicate polishing force control and smooth position/orientation control. The other is that



Fig. 17. Table with curved surface.

conventional and complicated teaching task is not required at all. When conventional sanding systems based on an industrial robot are used, desired trajectory for tool's position/orientation control is obtained through complicated teaching process. In this case, operator has to input a large number of teaching points along object's surface. However, the proposed robot sander directly handles CL data generated from 3D CAD/CAM, so that such a teaching process can be omitted. Experimentally, the sanding tool attached to the tip of the robot arm could smoothly follow the curved surface, keeping a contact from normal direction with a desired polishing force. It was also demonstrated that the proposed system could successfully sand the curved surface of attractive furniture with extremely good quality.

The process parameters such as sanding conditions and control gains given in the experiments were tuned with trial and error in consideration of efficiency and sanded surface quality, and worked well for the examples shown in this paper. However, if the robot sander is applied to other different materials, desirable parameters (i.e., semi-optimized parameters) should be found again. Because the desirable parameters tend to largely depend on the species of wooden material. In the future, we plan to accumulate a database that has promising relations between the species

of wooden material and desirable parameters. Though the parameters should be further tuned time-varyingly and delicately in compliance with intra species variations as well as directionality and changes in a single workpiece so as to realize an ideal robot sander, no practical on-line assessment techniques for wooden materials seem to be proposed yet at this stage.

References

- [1] Ozaki F, Jinno M, Yoshimi T, Tatsuno K, Takahashi M, Kanda M, et al. A force controlled finishing robot system with a task-directed robot language. *J Robotics Mechatronics* 1995;7(5):383–8.
- [2] Pfeiffer F, Bremer H, Figueiredo J. Surface polishing with flexible link manipulators. *Eur J Mech, A/Solids* 1996;15(1):137–53.
- [3] Takeuchi Y, Ge D, Asakawa N. Automated polishing process with a human-like dexterous robot. *Proceedings of IEEE international conference on robotics and automation*; 1993. p. 950–6.
- [4] Pagilla PR, Yu B. Robotic surface finishing processes: modeling, control, and experiments. *Trans ASME, J Dyn Syst Meas Control* 2001;123:93–102.
- [5] Huang H, Zhou L, Chen XQ, Gong ZM. SMART robotic system for 3D profile turbine vane airfoil repair. *Int J Adv Manuf Technol* 2003;21(4):275–83.
- [6] Stephien TM, Sweet LM, Good MC, Tomizuka M. Control of tool/workpiece contact force with application to robotic deburring. *IEEE J Robotics Autom* 1987;3(1):7–18.
- [7] Kazerooni H. Robotic deburring of two-dimensional parts with unknown geometry. *J Manuf Syst* 1988;7(4):329–38.
- [8] Her MG, Kazerooni H. Automated robotic deburring of parts using compliance control. *Trans ASME, J Dyn Syst Meas Control* 1991;113:60–6.
- [9] Bone GM, Elbestawi MA, Lingarkar R, Liu L. Force control of robotic deburring. *Trans ASME, J Dyn Syst Meas Control* 1991;113:395–400.
- [10] Gorinevsky DM, Formalsky AM, Schneider AYU. *Force control of robotics systems*. New York: CRC Press; 1997.
- [11] Hogan N. Impedance control: an approach to manipulation: Part I–Part III. *Trans ASME, J Dyn Syst Meas Control* 1985;107:1–24.
- [12] Raibert MH, Craig JJ. Hybrid position/force control of manipulators. *Trans ASME, J Dyn Syst Meas Control* 1981;102:126–33.
- [13] Takahashi K, Aoyagi S, Takano M. Study on a fast profiling task of a robot with force control using feedforward of predicted contact position data. *Proceedings of the fourth Japan–France Congress & second Asia–Europe Congress on Mechatronics*. 1998. p. 398–401.
- [14] Nagata F, Watanabe K, Sato K, Izumi K. An experiment on profiling task with impedance controlled manipulator using cutter location data. *Proceedings of IEEE international conference on systems, man, and cybernetics*, vol. IV; 1999. p. 848–53.
- [15] Nagata F, Watanabe K, Sato K, Izumi K. Generalized fuzzy environment models learned with genetic algorithms for a robotic force control. *Proceedings of the IEEE/RSJ international conference on intelligent robots and systems*; 1999. p. 590–6.
- [16] Nagata F, Kusumoto Y, Watanabe K, Tsuda K, Yasuda K, Murase Y. Development of an intelligent sanding machine for new designed furniture—3D robot sander with a contact force controller. *Proceedings of the 16th international wood machining seminar*; 2003. p. 546–52.
- [17] Nagata F, Watanabe K, Tsuda K, Kawaguchi S, Fujimoto Y, Murase Y. Performance test of a force controlled robot sander using a surface following controller based on cutter location data. *J Jpn Soc Precis Eng* 2002;68(7):953–7 [in Japanese].
- [18] Kusumoto Y, Nagata F, Watanabe K, Tsuda K, Yasuda K, Murase Y. Development of an intelligent sanding machine for new designed furniture—high quality sanding of 3D curved surface using hyper cutter location data. *Proceedings of the 16th international wood machining seminar*; 2003. p. 553–61.
- [19] Nagata F, Watanabe K, Izumi K. Profiling control for industrial robots using a position compensator based on cutter location data. *J Jpn Soc Precis Eng* 2000;66(3):473–7 [in Japanese].
- [20] Nagata F, Watanabe K, Izumi K. Furniture polishing robot using a trajectory generator based on cutter location data. *Proceedings of 2001 IEEE international conference on robotics and automation*; 2001. p. 319–24.
- [21] Craig JJ. *Introduction to robotics—mechanics and control*. 2nd ed. Reading, MA: Addison Wesley; 1989.